

Crack Propagation in Solder Joints During Thermal-Mechanical Cycling

Ronald G. Ross, Jr.

Liang-chi Wen

Jet Propulsion Laboratory,
4800 Oak Grove Dr.,
Mail Stop 233-105
Pasadena, CA 91109

Differential expansion induced creep-fatigue resulting from temperature cycling is an important cause of solder joint failure. The deterioration of solder joint integrity typically involves a sequential development of local stressing, microcracks, crack initiation and crack propagation, ultimately resulting in electrical open-circuiting by total joint separation from the PWB footprint. To better understand the failure process, a series of combined analytical and experimental investigations have been performed on flat-pack parts with gull-wing leads ranging in height from 9 to 56 mils. JPL's special purpose nonlinear finite element computer program has been modified to dynamically simulate the crack propagation process. Solder creep properties, including the effect of grain growth, are also incorporated into the model. Depending upon the system geometry and materials properties, the combination of crack development and grain growth may have either a positive or negative effect on the rate of cracking of the solder elements. Consequently, the crack propagation process may accelerate or decelerate as cycles progress. Sensitivity studies are used to highlight the individual effects of crack propagation and grain growth and compare the failure prediction results with those obtained using conventional finite element techniques. The analytical results are corroborated using visual observations obtained using SEM photography of test samples exposed to the thermal-cycle environment used in the analysis.

Introduction

In most electronic packaging applications it is not a single high stress event that breaks a component solder joint; rather it is repeated or prolonged load applications that result in crack propagation through creep-fatigue failure of the solder. The failure of the solder joint typically involves a sequential development of local stressing, micro-cracks, crack initiation and crack propagation, ultimately resulting in electrical open-circuiting by total joint separation from the PWB footprint.

From a functional point of view, the loss of service by electrical open-circuiting is the ultimate concern. As a result most analytical life prediction methodologies are based on the mean time to total failure. By far the most common life prediction algorithm is the Coffin-Manson relationship shown in Eq. (1) (Manson, 1965):

$$N_f^k \Delta\epsilon = C \quad (1)$$

where

N_f = the number of cycle to failure

k = the ductility exponent (~ 0.40)

$\Delta\epsilon$ = cyclic plastic strain range inc. creep strain

C = ductility coefficient (~ 0.80)

When Eq. (1) is used for life prediction it is common to compute the strain range ($\Delta\epsilon$) to be the total plastic strain range, including creep strain, in the highest strain portion of the solder joint. This provides a good prediction for solder joint cracking at the point of highest strain, but fails to include any crack propagation dynamics whereby the advancing crack may either accelerate, or arrest, depending on whether the crack presence increases or decreases the strain on the remaining parts of the solder joint. Because crack propagation can occur over many months or years, other time-dependent aging phenomena such as grain growth, oxidation, and formation of intermetallic layers may also influence the crack propagation dynamics, and thus the actual time, or cycles, to failure.

In addition to solder failure prediction, solder joint qualification and inspection are also particularly sensitive to crack propagation dynamics. Test verification and qualification pass/fail criteria for spacecraft and military hardware range from "initiation of solder joint cracking" to "presence of an electrical open circuit," depending upon the agency and mission. Example qualification criteria include the widely accepted MANTECH (1991) test requirement of "no electrical open circuits after 1000 cycles between -55°C and $+125^\circ\text{C}$," and the NASA (1986) requirement of no visible cracks after 200 cycles between -55°C and $+100^\circ\text{C}$.

The important issue linking both the failure-prediction al-

Contributed by the Electrical and Electronic Packaging Division and presented at the Winter Annual Meeting, New Orleans, LA, November 28-December 3, 1993 of THE AMERICAN SOCIETY OF MECHANICAL ENGINEERS. Manuscript received by the EEPD August 1, 1993. Paper No. 93-WA/EEP-9. Associate Technical Editor: J. H. Lau.

gorithms and the qualification test criteria is the complex dynamics of crack propagation. A key question is whether one can establish definitive correlations between “crack appearance” and “open-circuiting resulting from total separation,” and to what extent these correlations are dependent on component lead geometry and flexibility, and on metallurgical changes—particularly grain growth—in the solder during crack propagation. Understanding crack propagation dynamics and the parameter dependencies controlling crack propagation is important to both achieving robust electronic packaging designs that meet the end-use requirements, and to defining and interpreting appropriate accelerated testing and inspection procedures for hardware qualification.

Study Approach

In studying the crack propagation dynamics of solder joints, many important parameters such as dependence on component lead flexibility and interconnection geometry, dependence on solder metallurgical properties, and temperature dependence, are known to be heavily interrelated. With this background, the approach of the present study has been to utilize JPL’s special-purpose, nonlinear finite-element elastic-plastic-creep simulation program to model the behavior of solder crack propagation dynamics in the context of the complete part-lead-solder-PWB system. To better understand and corroborate the analytical modelling effort, a series of experimental investigations were also performed using flat-pack parts with gull-wing leads.

Finite Element Creep-Fatigue Simulation Modeling. The JPL-developed creep-fatigue finite element program is a true time-response simulation program whereby the time response of the solder joint is divided into thousands of consecutive time increments; for each time increment the solder’s incremental plastic strain response is computed based on the existing stress in the solder, the solder’s temperature and constitutive properties, the presence and level of any previously generated microcracks, and the state of externally applied loads. The program starts each time increment by computing the instantaneous stress in each solder element using a special-purpose finite element elastic structural model of the complete part-lead-solder-PWB system. The forcing function for the stresses is the instantaneous geometry of the package system including previously accrued plastic deformation of the solder elements and lead deflections applied externally by thermal-cycle differential expansions or mechanical (isothermal) cycling.

Following computation of the stress, the program uses measured constitutive properties of solder that model the dependency of solder strain rate on applied stress, temperature, and metallurgical properties. These are used together with the current solder temperature to compute the plastic strain rate in each solder element, and thus the solder incremental strain during the time interval. To include the effects of crack propagation, the program estimates the amount of crack growth in each solder element based on a modified Coffin-Manson correlation and Miner’s rule as described in the next section. The amount of crack growth in each solder element is in turn used to continuously update the mechanical properties of each solder finite element.

Dynamic Simulation of Crack Propagation. Mechanistically, the growth of micro-cracks decreases the effective cross-sectional area of each element of the solder joint in proportion to the extent of local crack formation. The area loss is manifested as a localized decrease in element stiffness, which interacts with the balance of the solder joint structural system in determining the magnitude of loads and strains applied to each element during the loading history. In the JPL finite element model the effective area of each solder element is dynamically reduced at the end of each loading cycle (*i*) in

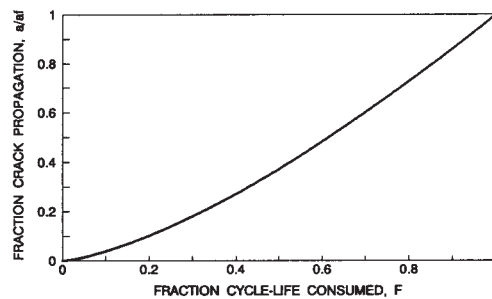


Fig. 1 Relationship between fraction of solder cross-sectional area cracked (a/a_i) and fraction of Coffin-Manson cycle-life consumed

proportion to the extent of localized cracking that develops within that element. The extent of localized cracking is computed based on the fraction (F) of the element’s cycle-life that has been consumed up to and including cycle (*i*).

The early work of Manson (1965) and Kitagawa (1978) is used to compute the dependence of the fraction cracking on the fraction cycle-life consumption. In these works, a power-law relationship is suggested to correlate crack growth rate (da/dN) and cycle strain-intensity factor range ($\Delta\epsilon \sqrt{a}$) as shown in Eq. (2)

$$da/dN = B(\Delta\epsilon\sqrt{a})^s \quad (2)$$

where

- da/dN = crack length growth per strain cycle
- a = crack length
- N = number of strain cycles
- $\Delta\epsilon$ = cyclic plastic strain range
- s = crack growth exponent

Strictly speaking, the crack growth correlation shown in Eq. (2) is a generalized form of the Coffin-Manson equation. If the stress-strain relationship remains unchanged for a solder element during the life span of thermal-mechanical cycling, Eq. (2) can be integrated, and the fraction crack propagation (a/a_f) is correlatable to the fraction cycle-life consumed ($F = N/N_f$) with the power-law relationship shown in Eq. (3).

$$(a/a_f) = (N/N_f)^m = F^m, \quad \text{where } m \approx 1.43 \quad (3)$$

Thus the crack length reaches completion ($a/a_f = 1$), when the number of straining cycles (N) is equal to the fatigue life (N_f). This power-law relationship between fraction crack length and fraction cycle-life consumed is used for each element of the finite element model, and is illustrated in Fig. 1.

Although there are many possible approaches to compute the fraction cycle-life consumed (F), the most straightforward technique is to use Miner’s rule, which assumes a linear summation of individual damage fractions (f_i) for each cycle, i.e.,

$$F = \sum f_i, \quad i = 1, N \quad (4)$$

For brevity, the fraction cycle-life consumed per cycle is generally shortened in this paper to “damage fraction per cycle,” or sometimes to just “damage fraction.” Assuming Miner’s rule in the context of cyclic fatigue, the damage fraction per cycle reduces to $1/N_f$, where N_f is the predicted number of cycles to failure for a particular strain-cycle depth. Appealing to Eq. (1) this gives

$$f_i = \text{damage fraction per cycle} = (\Delta\epsilon_i/C_i)^{1/k} \quad (5)$$

In this study the ductility coefficient (C) in Eq. (5) is also computed separately as a power-law function of maximum stress in the solder element during the *i*th cycle. This modification to the classical Coffin-Manson correlation was incorporated to approximate the known strain rate dependence of solder fracture.

For cases where a long-term creep-ratchet strain develops in

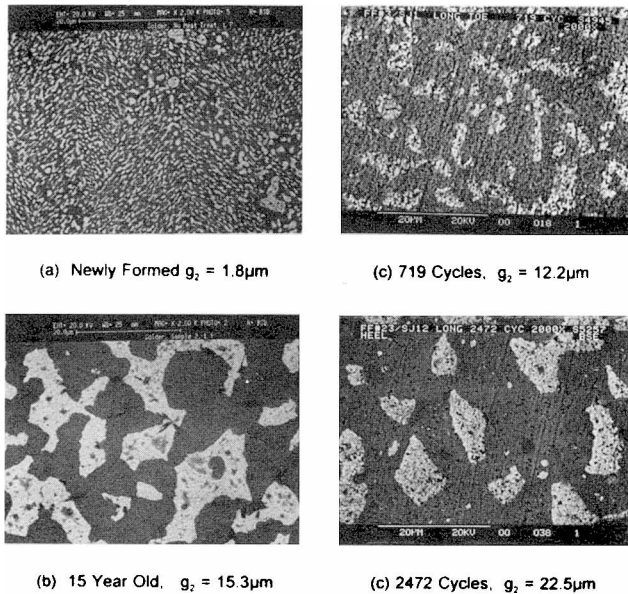


Fig. 2 SEM cross-sections of solder joints with various aging histories and exposures to -25°C to $+100^{\circ}\text{C}$ thermal cycles (dark regions are tin)

the solder joint, the fraction creep-rupture consumed during each loading cycle can be computed based on the work of Ross et al. (1992). Thus

$$f_i = \text{fraction creep-rupture life consumed per cycle} \\ = \delta(0.25)^k / C \quad (6)$$

where δ is the amount of creep ratcheting (shear or tension) between the $i - 1$ and the i th cycles, and C is the ductility coefficient from Eq. (1). It should be noted that creep ratcheting damage is for tension and shear only. Literature data (Manson et al., 1971) suggest that while tension creep ratcheting can be treated similar to monotonic straining, the damage from cyclic compression creep ratcheting produces no inter-crystalline cracking and is considered to be negligible.

In summary, for every solder element, the fraction cycle-life consumed in the i th cycle (f_i) is evaluated using Eqs. (5) and (6), and is summed to the previously consumed cycle-life fraction to obtain the total fraction cycle-life consumed (F). The fraction crack propagation within the element after i th cycle, $(a/a_f)_i$, is then computed using Eq. (3), as displayed in Fig. 1.

Dynamic Simulation of Solder Grain Growth. The second important time-dependent phenomena incorporated into the creep-fatigue simulation model is the effect of solder grain coarsening with long-term aging. Because of its low melting point (around 183°C), near-eutectic tin-lead solder alloy has a recrystallization temperature very close to room temperature. As a result, solid-state diffusion rates are high and the microstructure of solder continually coarsens, with grain size increasing monotonically during long-term aging or accelerated testing. Figure 2 illustrates the variation of solder joint microstructure from the very fine structure of newly formed solder joints, to the segregated large-grain structures of solder joints subjected to extended thermal-mechanical aging.

Figure 3 summarizes representative constitutive property data for the creep properties of solder as measured by Weinbel, et al. (1987), Avery and Backofen (1965), Zehr and Backofen (1968), Cline and Alden (1967), Murty (1973), and Kashyap and Murty (1981); the plot highlights the strong sensitivity of solder strain rate to applied stress and to the metallurgical condition of the solder. Notice that solder exhibits three distinct

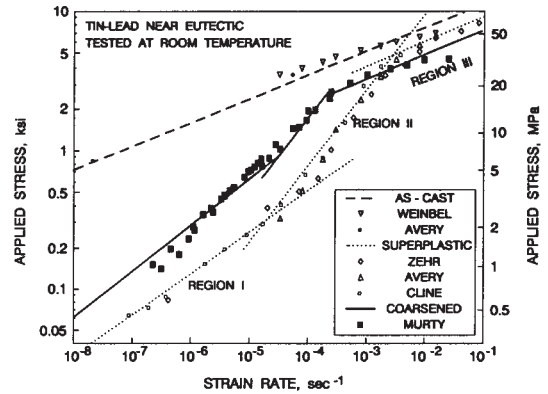


Fig. 3 Dependence of strain-rate on applied stress and metallurgical condition of room-temperature eutectic Sn-Pb solder

strain-rate slope behaviors depending on the stress and temperature level. Regions I and III are regions of classic metal plastic deformation, whereas Region II is a so-called region of superplastic behavior. In this superplastic region the solder is able to withstand much larger levels of deformation without rupture.

Within each of the three regions Arrowood et al. (1991) note that the creep behavior of solder is well approximated by Eq. (7). Note in Eq. (7) that increased grain size (increased g) restricts the strain rate and thus makes solder joints more resistant to failure under creep loading conditions (see Murty, 1973 and Kashyap and Murty, 1981).

$$\dot{\epsilon} \propto \sigma^n g^{-p} \exp(-Q/kT) \quad (7)$$

where

- $\dot{\epsilon}$ = solder strain rate, s^{-1}
- σ = solder stress
- n = creep exponent (typically $n = 2$ to 3)
- g = grain size
- p = grain size exponent (typically $p = 1.6$ to 2.3)
- Q = thermal activation energy of creep
- T = solder temperature (K)
- k = Boltzmann constant

The JPL finite element model uses an expanded version of Eq. (7) together with a semi-empirical relationship, based on experimental data, that predicts solder grain growth as a function of time and thermal exposure. This grain-growth model, presented as Eq. (8), is used to compute the grain size (g) that is used in the expanded version of Eq. (7).

$$\zeta = \zeta_o + \sum \Delta \zeta_i, \quad i = 1 \text{ to } N. \\ \Delta \zeta_i = (B^2 / \zeta_{i-1}) \exp(-E_g/kT_i) (t_i - t_{i-1}) \\ B = 375 (1 + 0.39(\sigma_{\text{avg}})^{1/2}) \\ g_i = g_o (l_i / l_o)^{1.5} \quad (8)$$

where

- ζ_i = grain growth ratio $(l_i - l_c) / l_c$ at time increment i
- ζ_o = initial grain growth ratio
- l_i = inter-granular distance at time increment i
- l_c = characteristic inter-granular distance
- l_o = initial inter-granular distance; $l_o / l_c = 3.45$
- g_i = grain size at time increment i
- g_o = initial grain size (planar metal. intercept length)
- σ_{avg} = solder stress during thermal-mechanical cycling, ksi
- E_g = activation energy for grain growth, 0.52eV
- k = Boltzmann constant: $8.63 \times 10^{-5} \text{ eV/K}$
- T_i = solder joint temperature at time increment i , K
- t_i = elapsed time from start to time increment i , hr

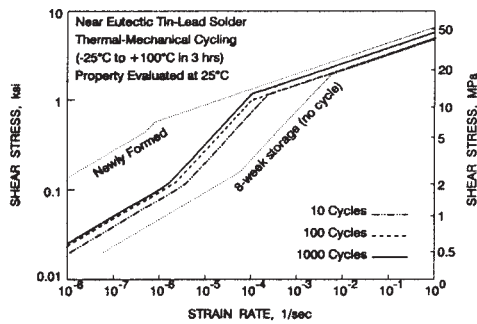


Fig. 4 Predicted changes in solder constitutive properties after exposure to numbers of 3-hr thermal-cycles from -25 to $+100^{\circ}\text{C}$

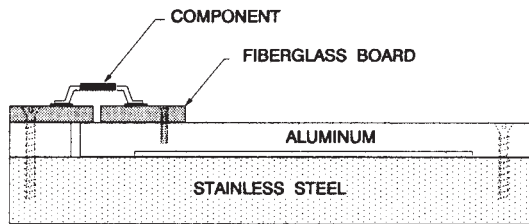


Fig. 5 JPL Bi-metal test fixture used for accelerated thermal-cycling of surface-mounted components

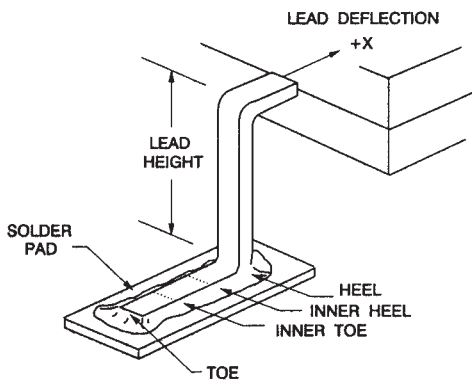


Fig. 6 Solder-joint nomenclature and dimension definitions for flat-pack parts mounted with gull-wing leads

In the analyses and experimental tests described in the remainder of this paper, a standard 3-hour thermal-cycle from -25°C to 100°C is used. Figure 4 summarizes the modeled room-temperature constitutive properties of solder that correspond to exposure to various numbers of these cycles. The dotted lines labeled as "newly formed" and "8-week storage" are the two reference states representing the hard brittle "as-cast" condition, and the ductile "age-softened" condition prior to cycling, respectively. It can be seen in Fig. 4 that after the initial softening period, the material gradually hardens with increasing number of cycles.

Experimental Testing. The experimental portion of this study utilized a special bi-metallic test board (Fig. 5) developed at JPL (Ross et al., 1991) to conduct accelerated thermal-cycle fatigue tests on flat-pack parts with gull-wing leads. Lead nomenclature and the lead loading deflection " X " are defined in Fig. 6.

A key advantage of the bimetal fixture, in addition to the high acceleration ratio, is the fact that it can be directly placed into the SEM for nondestructive microscopic examination of solder joint crack propagation status. Also, the relative position of the two metal plates (one aluminum with a CTE

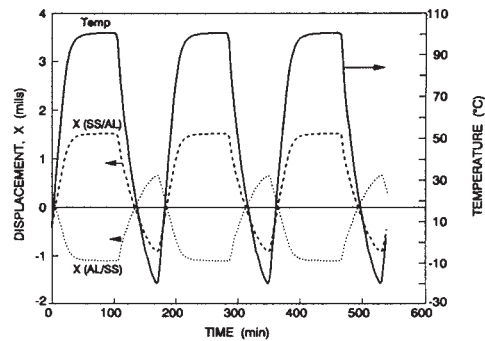


Fig. 7 Temperature-cycle profile and corresponding component lead deflections generated by the SS/AL and AL/SS test fixtures

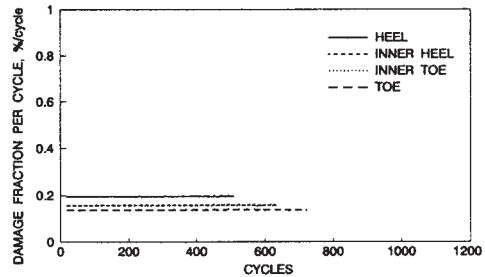


Fig. 8 Solder cycle-life consumption per cycle computed using conventional finite-element creep-fatigue simulation with no crack propagation or grain growth

around $23 \text{ ppm}/^{\circ}\text{C}$, the other 416 stainless steel with a CTE around $9 \text{ ppm}/^{\circ}\text{C}$) can be reversed.

During the tests, the boards were temperature-cycled using a 3-hour-per-cycle period with temperature ranging from -25°C to $+100^{\circ}\text{C}$. Figure 7 illustrates the variations of X and the temperature profile during the thermal cycle. It can be seen that for the SS/AL (the stainless plate on top of the aluminum plate) configuration, the displacement X is directly proportional to the temperature, and the total displacement range is 2.44 mils. On the other hand, if the two metal plates are reversed to obtain the AL/SS configuration, then the total displacement range is reduced to 1.75 mils, and the displacement (X) is 180 deg out of phase with the temperature profile.

The experiments and analyses of this study were primarily based on a TI SNJ54S22, M38510/07007BDB 14-lead flatpack. Lead heights, ranging from 9 to 62 mils, were die formed, and the parts were hand soldered to the PWB footprint using 63-37 Sn-Pb eutectic solder.

Crack Propagation and Grain Growth Sensitivity Study

In the following example, both the analysis and test involve a flatpack component with 38-mil-high gull-wing leads mounted on the SS/AL fixture and thermal cycled between -25°C and $+100^{\circ}\text{C}$. Dynamic simulations were performed with the crack propagation and grain growth algorithms both enabled and disabled to demonstrate the effects of these features.

No Crack Propagation or Grain Growth. In order to provide a baseline for interpreting the effects of the crack-propagation and grain-growth algorithms, the first analysis is conducted without these features enabled. With neither crack propagation nor grain growth present, the dynamic simulation reduces to a conventional finite element fatigue analysis with the fraction cycle-life consumed per cycle assumed to be constant. Figure 8 displays the fatigue predictions for four equally spaced points along the gull-wing foot: the heel, the inner heel, the inner toe, and the toe, as defined in Fig. 6. The total fraction

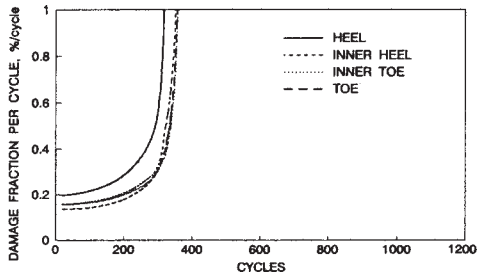


Fig. 9 Solder cycle-life consumption computed using simulation model with both crack propagation and grain-growth algorithms

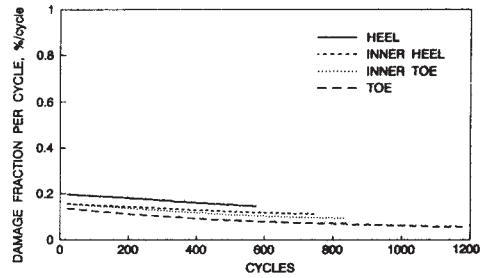


Fig. 12 Solder cycle-life consumption computed with grain-growth algorithm enabled, but with no crack propagation

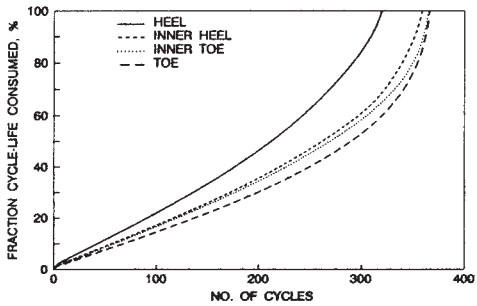


Fig. 10 Overall fatigue-failure dynamics computed with both crack propagation and grain-growth algorithms

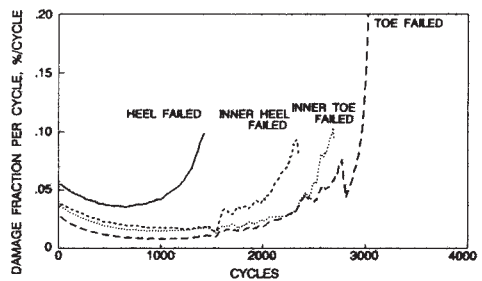


Fig. 13 Solder cycle-life consumption computed for flat-packs with highly flexible 56-mil-high gull-wing leads

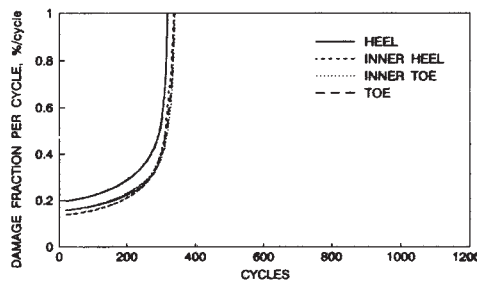


Fig. 11 Solder cycle-life consumption computed with crack propagation algorithm, but with the grain growth turned off

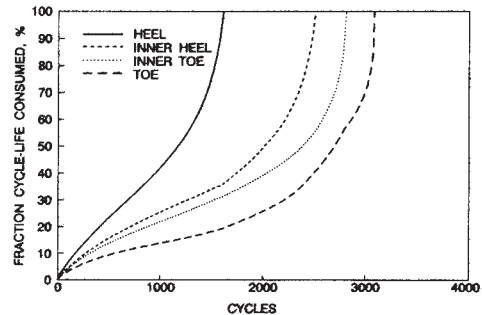


Fig. 14 Overall fatigue-failure dynamics computed for flat-packs with 56-mil-high leads

cycle-life consumed (F) is the integrated area under each curve; thus each solder element fails when its integral reaches a value of 100 percent. Note that this conventional Coffin-Manson analysis predicts that the heel will fail first, at 510 cycles, and the toe last, at 720 cycles. Although the solder joint is not failed open-circuit until the final element has failed—in this case the toe, many life predictions are based only on the highest stress region of the part—in this case the heel, which fails at 510 cycles.

Both Crack Propagation and Grain Growth. Figures 9 and 10 show the contrasting results based on the full crack propagation and grain-growth simulation. Note that total solder-joint fracture and separation is predicted after 366 cycles, and that the toe fails relatively quickly after the heel due the transfer of load toward the toe as the crack progresses from heel to toe. In the conventional Coffin-Manson analysis in Fig. 8, no provision for such a load transfer exists. Note also that the damage fractions gradually increase as the cracks propagate, eventually leading to rapid failure as the elements approach their end-of-life.

Crack Propagation, But No Grain Growth. To illuminate the effect of the grain growth part of the simulation, the above problem was re-analyzed with the crack propagation algorithm enabled, but with the grain growth algorithm turned off. Figure

11 shows the resulting simulation of crack propagation. Because the lack of grain growth leads to somewhat larger creep strains, the solder joint ruptures after 349 cycles, slightly sooner than in Fig. 10.

Grain Growth, But No Crack Propagation. Figure 12 illustrates the effect of eliminating the crack growth part of the algorithm, but keeping the grain growth active. Note that grain growth during the cycling results in a gradual reduction in the damage fraction per cycle over that shown in the conventional Coffin-Manson analysis in Fig. 8, and predicts a significantly prolonged life expectancy, near 1200 cycles.

In summary, the crack propagation process generally involves both grain growth and crack propagation. In the case of a part with compliant leads, the two factors have opposite effects. Consequently the acceleration or deceleration of crack propagation depends very much on which one of the two competing factors is the more influential.

Solder Crack Propagation With Highly Compliant Leads

With highly compliant leads, the overall strain level is significantly reduced and the role of tension/compression fatigue damage becomes more significant, especially at the heel. Figures 13 and 14 illustrate the computed failure trends for 56-

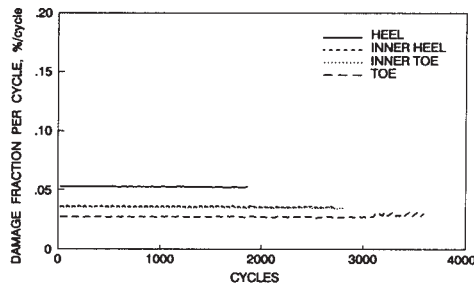


Fig. 15 Solder cycle-life consumption computed for 56-mil-high lead using conventional creep-fatigue simulation with no crack propagation or grain growth

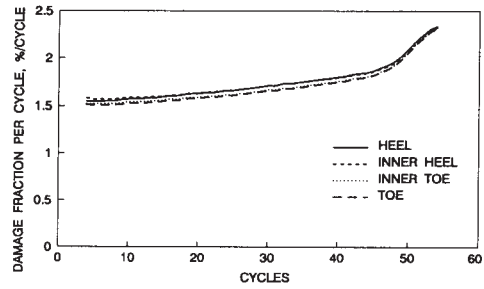


Fig. 17 Solder cycle-life consumption computed for flat-packs with short, stiff, 9-mil-high leads

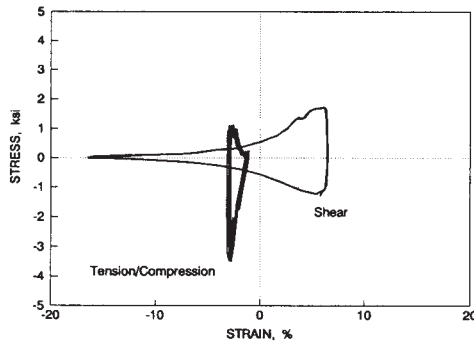


Fig. 16 Solder stress-strain hysteresis loops computed for flat-packs with stiff 9-mil-high gull-wing leads

mil-high gull-wing leads thermal cycled on the SS/AL fixture. Note that the rate of damage accumulation first decelerates due to the hardening effect of grain growth, and then accelerates as the crack propagation becomes more prominent. The model predicts that the heel is completely separated from the pad after about 1500 cycles, when the toe crack has only progressed ~ 10 percent. Total toe separation is predicted to occur much later at 3083 cycles.

At the end of the simulation, the grain growth model predicts a grain growth ratio, ζ^* = 16.3, which corresponds to a grain size ratio (g_i/g_o) of 12; thus, the grain size has grown to 12 times the initial size of 1.8 microns. This computed grain growth agrees quite well with the observations shown in Fig. 2. In addition, the computed crack propagation trends also agree quite well with the experimental observations.

In contrast to the crack propagation and grain growth model results, Fig. 15 presents the corresponding life prediction using the conventional model that assumes constant damage fraction per cycle.

Fracture Dynamics During Fast Fracture

When a gull-wing flat-pack is attached with short leads, solder-joint strain tends to be dominated by shear strain that runs from heel to toe, parallel to the circuit board. To explore the crack dynamics of this situation, the simulation model was run for a flat-pack mounted on the AL/SS board with short 9-mil-high leads and thermal cycled from -25°C to $+100^\circ\text{C}$ as before. Figure 16 displays the cyclic stress-strain loops computed by the finite-element model for the heel of the solder joint at the time of the 10th thermal cycle. Note that the horizontal shear strain range is around 23 percent, while the strain range in the normal-to-the-board tension-compression direction is only about 1.7 percent. This corresponds to a fatigue life projection ($1/f_i$) of 64 cycles for the heel element.

The full crack propagation simulation results, shown in Fig. 17, predict the fracture of all solder elements after 55 cycles. Because shear straining dominates the creep-fatigue damage,

the damage accumulation at the heel and toe are almost the same. Thus, the failure process is governed mainly by uniform micro-crack growth throughout the solder joint. Since the entire failure process takes place within a few days, the change in solder mechanical properties due to grain growth is relatively minor. Because of these special conditions, the life projection based on the conventional model (i.e., 64 cycles) is quite close to that (55 cycles) based on the full dynamic simulation with crack propagation and grain growth.

Implications for Solder-Joint Failure Inspection

As pointed out in the introduction, crack appearance and percent of peripheral crack extension are often used as qualitative indicators of solder joint wear-out damage. An important issue in inspecting solder joint fatigue damage is the correlation between crack initiation, or a particular level of crack propagation, and the ultimate service life of the solder joint. The simulation results presented in the previous sections of this paper provide insight into the general dynamics of crack propagation, and agree quite well with visual observations made as part of the parallel experimental test program. An important issue confirmed by both the analysis and the test results is the fact that the time between first cracking at the heel and final cracking at the toe is highly dependent on the flexibility of the part/lead/PWB system. As flexibility increases, the ratio of the time to ultimate failure, to the time to crack initiation, also increases.

Because the crack propagation simulation delineates the stages of damage in terms of percent cracking in each portion of the solder joint, it is possible to exploit the results to assist in correlating crack appearance with assessments of fatigue life. Two observations made as part of this study include:

(1) A distinct crack can first be visually detected on each portion of the solder joint (heel, inner heel, inner toe and toe) approximately the time the predicted fraction cracking (a/a_f) reaches 5 to 8 percent for that portion.

(2) A relatively consistent correlation between fraction toe cracking and total separation was observed: after the fraction toe cracking reaches 5 to 8 percent, approximately 20 to 30 percent of the solder joint service life is consumed.

Based on these two observations, a useful damage signature for a solder joint with a gull-wing lead is as follows: when a distinct crack line is clearly observed at the toe (generally as a result of crack propagation from the heel along the side, covering approximately 3/4 of the length), approximately 1/3 of the solder joint service life has been consumed.

Summary Discussion

In all of the cases in this investigation—including fast fracture dominated by shear fatigue, and very slow propagation with significant microstructural changes—the predictions of total separation and stages of crack propagation are very close to the experimental results. This good correlation is the result of both careful modeling of the physics of solder failure, and

careful calibration of the models against previous JPL experimental test results.

Adding crack propagation and grain growth into the simulation model provides improved fidelity and visibility into the fracture process, but at a modest price of slower computer execution. The key change is that the crack propagation model must be run until ultimate failure is reached, sometimes requiring the simulation of thousands of thermal cycles. In the conventional JPL simulation model, the run can be stopped whenever a stable equilibrium strain range is reached; failure is then projected using the conventional assumption of linearly increasing damage with increasing numbers of cycles.

As seen in the included figures, the difference between the conventional fatigue analysis and the full analysis with crack propagation and grain growth is important, but not so large as to invalidate the utility of the conventional analysis. One of the most valuable features of the full analysis has proven to be its ability to illuminate and calibrate the output of the conventional fatigue analysis.

Acknowledgment

The work described in this paper was carried out by the Jet Propulsion Laboratory, California Institute of Technology, under contract with the National Aeronautics and Space Administration. The authors would like to especially thank Ms. Elizabeth Jetter who generated most of the figures used in this chapter, R. Scott Leland, who fabricated the Bi-Metal fixtures used in the experiment, Dr. John Winslow and Jack Kovak, who provided information and components used in the work herein, and Ken Evens for the preparation of samples and subsequent photography using Scanning Electron Microscopy.

References

- Arrowood, R., Mukherjee, A., and Jones, W. B., 1991, "Hot Deformation of Two Phase Mixtures," *Solder Mechanics: A State of the Art Assessment*, Minerals, Metals and Materials Society, Warrendale PA, pp. 107-153.
- Avery, D. H., and Backofen, W. A., 1965, "A Structural Basis for Superplasticity," *Trans. ASME*, Vol. 58, pp. 551-562.
- Cline, H. E., and Alden, T. H., 1967, "Rate Sensitive Deformation in Tin-Lead Alloy," *Trans. ASME*, Vol. 239, pp. 710-714.
- Kashyap, B. P., and Murty, G. S., 1981, "Experimental Constitutive Relations for the High Temperature Deformation of a Pb-Sn Eutectic Alloy," *Materials Science and Engineers*, Vol. 50, pp. 205-213.
- Kitagawa, H., Takahashi, S., Suh, C. M., and Miyashita, S., 1978, "Quantitative Analysis of Fatigue Process—Microcracks and Slip Lines under Cyclic Strains," *Fatigue Mechanisms*, Proc. of an ASTM-NBS-NSF Symposium, Kansas City, MO., May 1978, J. T. Fong, ed., ASTM STP 675, pp. 420-449.
- Manson, S. S., 1965, "Fatigue: A Complex Subject—Some Simple Approximations," *Engineering Mechanics*, Vol. 5, pp. 193-226.
- Manson, S. S., Halford, G. R., and Spera, D. A., 1971, "The Role of Creep in High Temperature Low Cycle Fatigue," *Advances in Creep Design*, Smith, A. I. ed., John Wiley & Sons, Chapter 12, pp. 229-249.
- MANTECH for Advanced Data/Signal Processing, 1991, WRDC-TR-89-8025.
- Murty, G. S., 1973, "Stress Relaxation in Superplastic Materials," *Journal of Material Science*, Vol. 8, pp. 611-614.
- NASA, 1986, *Requirements for Soldered Electrical Connections*, NHB 5300.4(3A-1), revalidated date June 1986.
- Ross, R. G., Jr., et al., 1991, "Creep-Fatigue Behavior of Microelectronic Solder Joints," *Proceedings of the 1991 MRS Spring Meeting*, Anaheim CA, April, 1991.
- Ross, R. G., Jr., Wen, L. C., Mon, G. R., and Jetter, E., 1992, "Creep-Fatigue Interactions with Flexible Lead Parts," *ASME JOURNAL OF ELECTRONIC PACKAGING*, Vol. 114, No. 2, June, pp. 185-192.
- Weinbel, R. C., Tien, J. K., Pollaak, R. A., and Kang, S. K., 1987, "Creep-Fatigue Interaction in Eutectic Lead-Tin Solder Alloy," *Journal of Material Science Letter*, Vol. 6, pp. 3091-3096.
- Wen, L. C., Mon, G. R., Jetter, E. S., and Ross, R. G., Jr., 1992, "Metalurgical Variations in Near Eutectic Tin-Lead Solder During Thermal-Mechanical Processes," JPL D-9632.
- Zehr, S. W., and Backofen, W. A., 1968, "Superplasticity in Lead-Tin Alloys," *Trans. ASME*, Vol. 61, pp. 300-312.